Multi-target Localization Using Frequency Diverse Coprime Arrays with Coprime Frequency Offsets

Si Qin [†], Yimin D. Zhang [‡], Moeness G. Amin [†]

[†] Center for Advanced Communications, Villanova University, Villanova, PA 19085, USA
[‡] Department of Electrical and Computer Engineering, Temple University, Philadelphia, PA 19122, USA

***Abstract*—The performance of the frequency diverse array (FDA) radar is fundamentally limited by the geometry of the array and the frequency offset. In this paper, we overcome this limitation by introducing a novel sparsity-based multi-target localization approach incorporating both coprime array and coprime frequency offset. The covariance matrix of the received signals corresponding to all sensors and employed frequencies is formulated to generate a space-frequency virtual difference coarrays. The proposed approach enables the localization of up to $\mathcal{O}(M^2N^2)$ targets using $\mathcal{O}(M+N)$ physical sensors with $\mathcal{O}(M+N)$ frequencies for a coprime pair of M and N. The joint DOA and range estimation is cast as a sparse reconstruction problem and solved using the complex multi-task Bayesian compressive sensing technique.**

***Index Terms*—Target localization, frequency diverse array radar, coprime array, coprime frequency offset, Bayesian compressvie sensing**

I. Introduction

Target localization finds a variety of applications in radar, sonar, communication, and navigation [1]–[4]. Localization implies range, angle, or both [5]–[7]. In this paper, target location is determined using the direction-of-arrival (DOA) and range information. In recent years, simultaneous localization of multiple targets has been rigorously investigated using array processing and multiple-input multiple-output (MIMO) systems (e.g., [8]–[10]). Among existing techniques, the frequency diverse array (FDA) is considered attractive due to its simplicity and effectiveness [11]. An FDA radar uses a small frequency increment across array elements, as compared with the carrier frequency, which results in beam steering as a function of the angle and range in the far field [12]–[14]. As a result, the DOA and range information can be jointly estimated. However, the localization performance is fundamentally limited by the geometry of the array and the design of frequency offsets. In essence, the resolutions in the angle and range domains are, respectively, determined by the array aperture and maximum frequency increment. Further, the number of degrees-of-freedom (DOFs) offered by the array sensors and frequency increments determines the maximum number of detectable targets. As a consequence, the conventional FDA radar with N-element uniform linear array (ULA) and uniform frequency increment can only localize up to $\mathcal{O}(N^2)$ targets, with a resolution $\mathcal{O}(1/N)$ in the angle and range domains, respectively.

Compared with ULA, sparse arrays use the same number of sensors to achieve a larger array aperture. They improve mainbeam properties and, thereby, provide enhanced performance in terms of angular accuracy and resolution. These attributes are achieved without any increase in size, weight, power consumption, or cost. In addition, sparse arrays offer a higher number of DOFs through the exploitation of the coarray concept [15] and, as such, increases the number of detectable targets. Likewise, non-uniform frequency offsets can be used to achieve improved estimation and sensing performance [16]. Among a number of techniques that are available for sparse signal structures and array aperture synthesis, the recent proposed coprime configurations offer systematical design capability and DOF analysis involving sensors, samples, or frequencies [19]–[27].

In this paper, we consider the target localization problem using an FDA radar, which incorporates both coprime array structure and coprime frequency offsets. The joint DOA and range estimation is cast as a sparse reconstruction problem and solved in the context of the compressive sensing (CS) techniques [28]. In the proposed approach, the offsets of carrier frequencies assume coprime values to further increase the number of DOFs beyond that achieved by only implementing the coprime arrays with uniform frequency increments. The covariance matrix of the received signals corresponding to all sensors and sensing frequencies is formulated to generate a space-frequency virtual difference coarrays. It is shown that the proposed approach enables the localization of up to $\mathcal{O}(M^2N^2)$ targets, with a resolution $\mathcal{O}(1/MN)$ in both angle and range domains, if $\mathcal{O}(M+N)$ physical sensors and $\mathcal{O}(M+N)$ frequencies are used for a coprime pair of M and N.

The target sparsity in range and angle is utilized by applying sparse reconstruction techniques which fully utilize all DOFs of the FDA. As a preferred approach, we use CS algorithms in the sparse Bayesian learning context as they achieve superior performance and are insensitive to the coherence of dictionary entries. To handle the complex-valued observations in the underlying problem, the complex multitask Bayesian compressive sensing (CMT-BCS) [30] is used. The CMT-BCS achieves improved sparse signal reconstruction because by utilizing the group sparsity of the real and imaginary components.

Notations: We use lower-case (upper-case) bold characters

This work was supported by the Office of Naval Research under Grant No. N00014-13-1-0061.

to denote vectors (matrices). In particular, $\mathbf{I}_N$ denotes the $N \times N$ identity matrix. $(.)^*$ implies complex conjugation, whereas $(.)^T$ and $(.)^H$ respectively denote the transpose and conjugate transpose of a matrix or vector. $\mathrm{vec}(\cdot)$ denotes the vectorization operator that turns a matrix into a vector by stacking all columns on top of the another, and $\mathrm{diag}(\mathbf{x})$ denotes a diagonal matrix that uses the elements of $\mathbf{x}$ as its diagonal elements. $\mathrm{E}(\cdot)$ is the statistical expectation operator and $\otimes$ denotes the Kronecker product. $P_r(\cdot)$ denotes the probability density function (pdf), and $\mathcal{N}(x|a,b)$ denotes that random variable x follows a Gaussian distribution with mean a and variance b. $\mathcal{CN}(a,\mathbf{R})$ denotes joint complex Gaussian distribution with mean a and covariance matrix $\mathbf{R}$. $\mathrm{Re}(x)$ and $\mathrm{Im}(x)$ denote the real and imaginary parts of complex element x, respectively.

II. Signal model

Without loss of generality, we limit our discussion to far-field targets in the two-dimensional (2-D) space where the DOA is described by the azimuth angle only. Extension to three-dimensional (3-D) space is straightforward.

As shown in Fig. 1, an FDA radar utilizes a coprime pair of uniform linear subarrays, i.e., $2M$-element subarray with an interelement spacing of N units, and N-element subarray with an interelement spacing of M units [18]. The unit interelement spacing is denoted as $d = \lambda_0/2 = c/(2f_0)$, where c is the velocity of electromagnetic wave propagation and f_0 is the carrier frequency. The two integers M and N are chosen to be coprime ($M < N$), i.e., their greatest common divisor is one. Define

$$\mathbb{P} = \{Mn|0 \le n \le N-1\} \bigcup \{Nm|0 \le m \le 2M-1\} \quad (1)$$

as the union of two sparsely sampled integer subsets. Because the two subsets share the first element, the total number of entries in $\mathbb{P}$ is $2M+N-1$. Denote $\mathbf{p} = [p_1 d, ..., p_{2M+N-1} d]^T$ as the positions of the array sensors where $p_k \in \mathbb{P}$, $k = 1, ..., 2M+N-1$. The first sensor, located at $p_1 d = 0$, is assumed as the reference.

Consider a scene with Q far-field targets whose locations are modeled as (θ_q, R_q), $q = 1, 2, \cdots, Q$. Each FDA element radiates an incremental carrier frequency. That is, a continuous-wave (CW) signal transmitted from the kth element is expressed as

$$s_k(t) = \exp(j2\pi f_k t), \quad (2)$$

where radiation frequency $f_k = f_0 + \xi_k \Delta f$ is exploited with a unit frequency increment Δf, and ξ_k is an integer coefficient of the frequency offset applied at the kth element for $k = 1, ..., 2M+N-1$. In this paper, the FDA radar is operated with coprime frequency offsets, $\xi_k \in \mathbb{P}$, $k = 1, ..., 2M+N-1$. In addition, the maximum increment is assumed to satisfy $(2M+N-1)\Delta f \ll f_0$ so as to guarantee that the FDA radar works in a narrowband platform.

For a CW waveform with frequency f_k transmitted from the kth sensor, the signal received at the lth sensor is modeled as

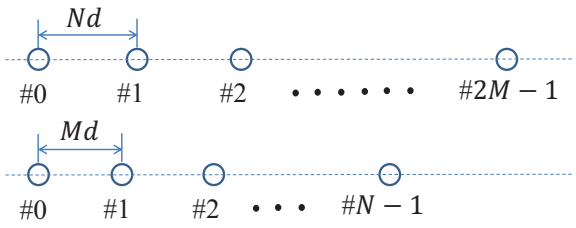

Fig. 1. The coprime array configuration.

$$\begin{aligned}\check{x}_{k,l}(t) =& \exp(j2\pi f_k t) \sum_{q=1}^{Q} \rho_q(t) e^{-j\frac{4\pi}{\lambda_k} R_q} e^{-j\frac{2\pi p_l d}{\lambda_k}\sin(\theta_q)} \\ &+ \check{n}_{k,l}(t), \quad k,l = 1, \ldots, 2M+N-1, \end{aligned} \quad (3)$$

where $\rho_q(t), q = 1, \ldots, Q$, are complex scattering coefficients of the targets, which are assumed to be uncorrelated zero-mean random variables with $E[\rho_q^* \rho_p] = \sigma_q^2 \delta_{q,p}, 1 \le q, p \le Q$, due to, e.g, the radar cross section (RCS) fluctuations. In addition, $\lambda_k = c/f_k$ denotes the wavelength corresponding to f_k. Furthermore, $\check{n}_{k,l}(t)$ is the additive noise, which is assumed to be spatially and temporally white, and are independent of target signals.

The received signal is converted to baseband signals corresponding to the respective frequencies, followed by low-pass filtering, yielding

$$\begin{aligned} x_{k,l}(t) =& \sum_{q=1}^{Q} \rho_q(t) e^{-j\frac{4\pi}{\lambda_k} R_q} e^{-j\frac{2\pi p_l d}{\lambda_k}\sin(\theta_q)} + n_{k,l}(t) \\ =& \sum_{q=1}^{Q} \rho_q(t) e^{-j\frac{4\pi f_k}{c} R_q} e^{-j\frac{\pi p_l f_k}{f_0}\sin(\theta_q)} + n_{k,l}(t), \end{aligned} \quad (4)$$

where $n_{k,l}(t)$ is the noise at the filter output with a variance σ_n^2. Note that $f_k/f_0 = (f_0 + \xi_k \Delta f)/f_0 \approx 1$, due to the increment $\xi_k \Delta f \ll f_0$. Then, (4) can be expressed as

$$x_{k,l}(t) = \sum_{q=1}^{Q} \rho_q(t) e^{-j\frac{4\pi f_k}{c} R_q} e^{-j\pi p_l \sin(\theta_q)} + n_{k,l}(t). \quad (5)$$

Stacking all $x_{k,l}(t)$ for $k, l = 1, ..., 2M+N-1$, yields a $(2M+N-1)^2 \times 1$ vector,

$$\begin{aligned} \mathbf{x}(t) =& \sum_{q=1}^{Q} \rho_q(t) \mathbf{a}_{p,f}(\theta_q, R_q) + \mathbf{n}(t) \\ =& \mathbf{A}_{p,f} \mathbf{d}(t) + \mathbf{n}(t), \end{aligned} \quad (6)$$

where $\mathbf{a}_{p,f}(\theta_q, R_q) = \mathbf{a}_p(\theta_q) \otimes \mathbf{a}_f(R_q)$ represents the steering vector related to the angle-range pair (θ_q, R_q). Herein, $\mathbf{a}_p(\theta_q)$ and $\mathbf{a}_f(R_q)$ are steering vectors corresponding to θ_q and R_q, respectively, expressed as

$$\mathbf{a}_p(\theta_q) = \left[1, e^{-j\pi p_2 \sin(\theta_q)}, \cdots, e^{-j\pi p_{2M+N-1}\sin(\theta_q)}\right]^T, \quad (7)$$

$$\mathbf{a}_f(R_q) = \left[e^{-j\frac{4\pi f_1}{c} R_q}, e^{-j\frac{4\pi f_2}{c} R_q}, \cdots, e^{-j\frac{4\pi f_{2M+N-1}}{c} R_q}\right]^T. \quad (8)$$

In addition, $\mathbf{A}_{p,f} = [\mathbf{a}_{p,f}(\theta_1), \cdots, \mathbf{a}_{p,f}(\theta_Q)]$ and $\mathbf{d}(t) = [\rho_1(t), \cdots, \rho_Q(t)]^T$, and $\mathbf{n}_k(t)$ is the noise vector following the complex Gaussian distributions $\mathcal{CN}(0, \sigma_n^2 \mathbf{I}_{(2M+N-1)^2})$.

The $(2M+N-1)^2 \times (2M+N-1)^2$ covariance matrix of data vector $\mathbf{x}(t)$ is obtained as

$$\begin{aligned}\mathbf{R}_{\mathbf{x}} &= \mathrm{E}[\mathbf{x}(t)\mathbf{x}^H(t)] = \mathbf{A}_{p,f}\mathbf{R}_{\mathbf{dd}}\mathbf{A}_{p,f}^H + \sigma_n^2\mathbf{I}_{(2M+N-1)^2} \\ &= \sum_{q=1}^{Q} \sigma_q^2 \mathbf{a}_{p,f}(\theta_q, R_q)\mathbf{a}_{p,f}^H(\theta_q, R_q) + \sigma_n^2\mathbf{I}_{(2M+N-1)^2},\end{aligned} \tag{9}$$

where $\mathbf{R}_{\mathbf{dd}} = \mathrm{E}[\mathbf{d}(t)\mathbf{d}^H(t)] = \mathrm{diag}([\sigma_1^2, \ldots, \sigma_Q^2])$ represents the target scattering power. Note that we assume the target scattering coefficients to be frequency-independent for the emiting signals because the frequency offsets are small. In practice, the covariance matrix is estimated using T available samples, i.e.,

$$\hat{\mathbf{R}}_{\mathbf{x}} = \frac{1}{T}\sum_{t=1}^{T} \mathbf{x}(t)\mathbf{x}^H(t). \tag{10}$$

By vectorizing the matrix $\hat{\mathbf{R}}_{\mathbf{x}}$, we obtain the following $(2M+N-1)^4 \times 1$ measurement vector:

$$\mathbf{z} = \mathrm{vec}(\hat{\mathbf{R}}_{\mathbf{x}}) = \tilde{\mathbf{A}}_{p,f}\mathbf{b}_{p,f} + \sigma_n^2\tilde{\mathbf{i}}, \tag{11}$$

with

$$\tilde{\mathbf{A}}_{p,f} = [\tilde{\mathbf{a}}_{p,f}(\theta_1, R_1), \cdots, \tilde{\mathbf{a}}_{p,f}(\theta_Q, R_Q)], \tag{12}$$

$$\mathbf{b}_{p,f} = [\sigma_1^2, \cdots, \sigma_Q^2]^T, \tag{13}$$

$$\tilde{\mathbf{i}} = \mathrm{vec}\left(\mathbf{I}_{(2M+N-1)^2}\right), \tag{14}$$

where

$$\begin{aligned}\tilde{\mathbf{a}}_{p,f}(\theta_q, R_q) &= \mathbf{a}_{p,f}^*(\theta_q, R_q) \otimes \mathbf{a}_{p,f}(\theta_q, R_q) \\ &= \mathbf{a}_p^*(\theta_q) \otimes \mathbf{a}_f^*(R_q) \otimes \mathbf{a}_p(\theta_q) \otimes \mathbf{a}_f(R_q) \\ &= (\mathbf{a}_p^*(\theta_q) \otimes \mathbf{a}_p(\theta_q)) \otimes (\mathbf{a}_f^*(R_q) \otimes \mathbf{a}_f(R_q)) \\ &= \tilde{\mathbf{a}}_p(\theta_q) \otimes \tilde{\mathbf{a}}_f(R_q)\end{aligned} \tag{15}$$

for $1 \le q \le Q$. Benefiting from the Vandermonde structure of $\mathbf{a}_p(\theta_q)$ and $\mathbf{a}_f(R_q)$, the entries in $\tilde{\mathbf{a}}_p(\theta_q)$ and $\tilde{\mathbf{a}}_f(R_q)$ are still in the forms of $e^{-j\pi(p_i-p_j)\sin(\theta_q)}$ and $e^{-j4\pi(\xi_i-\xi_j)\Delta f R_q/c}$, for $i, j = 1, \cdots, 2M+N-1$. As such, we can regard $\mathbf{z}$ as a received signal from a single snapshot signal vector $\mathbf{b}_{p,f}$ and the matrix $\tilde{\mathbf{A}}_{p,f}$ corresponds to a higher number of virtual array sensors and virtual frequency offsets which are located at the lags between the two subarrays and two frequencies, respectively. As a consequence, the problem is similar to handling fully 2-D coherent targets, and some covariance matrix based techniques can be applied, e.g., the Fourier-based power spectrum density (PSD) [31] and MUSIC with spatial smoothing [32]. There are $\mathcal{O}(MN)$ available DOFs in $\mathbf{a}_p(\theta_q)$ and $\mathbf{a}_f(R_q)$, respectively. As such, the increased number of DOFs enables localization of far more targets. Provided that sufficient snapshots are available for reliable covariance matrix estimation, $\mathcal{O}(M^2N^2)$ angle-range pairs can be identified correctly.

Remark: The DOA and range information is contained in the phase term, which are wrapped within the $[-\pi, \pi)$ or $[0, 2\pi)$ range. It implies ambiguity in range due to phase wrapping. Therefore, the unambiguous range of localization of targets are given by $-90^\circ \le \theta_q < 90^\circ$ and $0 \le R_q < R_{\max} = c/(2\Delta f)$, for $q = 1, \cdots, Q$.

III. Target localization using CMT-BCS

The signal vector $\mathbf{z}$ in Eqn. (11) can be sparsely represented over the entire discretized angular girds as

$$\mathbf{z} = \mathbf{\Phi}\mathbf{r}, \tag{16}$$

where $\mathbf{\Phi} = \left[\mathbf{\Phi}_s, \tilde{\mathbf{i}}\right]$. Herein, $\mathbf{\Phi}_s$ is defined as the collection of steering vectors $\tilde{\mathbf{a}}_{p,f}(\theta_{g_1}, R_{g_2})$ over all possible grids θ_{g_1} and R_{g_2}, $g_1 = 1, \ldots, G_1, g_2 = 1, \ldots, G_2$, with $G = G_1G_2 \gg Q$. In addition, the vector $\mathbf{r}$ contains coefficients in these search grids to be determined. It is important to note that $\mathbf{r}$ is sparse, where the joint angle-range of targets, $(\theta_q, R_q), q = 1, \ldots, Q$, are indicated by positions of the nonzero entries. Thus, the problem described in (16) can be solve using sparse reconstruction techniques [33]–[37]. In this paper, we exploit the sparse Bayesian learning methods due to their superior performance and robustness to dictionary coherence. In particular, the CMT-BCS approach [30] is used to deal with complex entries.

Assume that the entries in sparse vectors $\mathbf{r}$ are drawn from the product of the following zero-mean Gaussian distributions:

$$\mathbf{r}_g \sim \mathcal{N}(\mathbf{r}_g|\mathbf{0}, \alpha_g\mathbf{I}_2), g \in [1, \ldots, G], \tag{17}$$

where $\mathbf{r}_g$ is a vector consisting of the real part coefficient r_{g_R} and imagery part coefficient r_{g_I} with respect to the gth grid in $\mathbf{r}$. In addition, $\boldsymbol{\alpha} = [\alpha_1, \ldots, \alpha_G]^T$ is the variance of Gaussian pdf. It is easy to confirm that $\mathbf{r}_g$ trends to be zero when α_g is set to zero [35].

To encourage the sparsity of $\mathbf{r}$, a Gamma prior is placed on α_g^{-1}, which is conjugate to the Gaussian distribution,

$$\alpha_g^{-1} \sim \mathrm{Gamma}(\alpha_g^{-1}|a, b), g \in [1, \ldots, G], \tag{18}$$

where $\mathrm{Gamma}(x^{-1}|a, b) = \Gamma(a)^{-1}b^a x^{-(a-1)}e^{-\frac{b}{x}}$, with $\Gamma(\cdot)$ denoting the Gamma function. It has been demonstrated in [38] that a proper choice of the hyper-parameters a and b encourages a sparse representation for the coefficients in $\mathbf{r}$. A Gaussian prior $\mathcal{N}(\mathbf{0}, \beta_0\mathbf{I}_2)$ is also placed on the additive noise. Similarly, the Gamma prior is placed on β_0^{-1} with hyper-parameters c and d.

The CMT-BCS algorithm carries out Bayesian inference by the Gibbs samplers [30]. Define $\hat{\mathbf{r}}_{RI} = \left[(\hat{\mathbf{r}}_R)^T, (\hat{\mathbf{r}}_I)^T\right]^T$ with $\hat{\mathbf{r}}_R = [\hat{r}_{1R}, \ldots, \hat{r}_{GR}]^T$ and $\hat{\mathbf{r}}_I = [\hat{r}_{1I}, \ldots, \hat{r}_{GI}]^T$. Then,

$$\Pr(\hat{\mathbf{r}}_{RI}|\mathbf{z}, \mathbf{\Phi}, \boldsymbol{\alpha}, \beta_0) = \mathcal{N}(\hat{\mathbf{r}}_{RI}|\boldsymbol{\mu}, \mathbf{\Sigma}), \tag{19}$$

where

$$\mathbf{z}_{RI} = [\mathrm{Re}(\mathbf{z})^T, \mathrm{Im}(\mathbf{z})^T]^T \tag{20}$$

$$\boldsymbol{\mu} = \beta_0^{-1}\mathbf{\Sigma}\mathbf{\Psi}^T\mathbf{z}_{RI}, \tag{21}$$

$$\mathbf{\Sigma} = \left[\beta_0^{-1}\mathbf{\Psi}^T\mathbf{\Psi} + \mathbf{F}^{-1}\right]^{-1}, \tag{22}$$

$$\mathbf{\Psi} = \begin{bmatrix}\mathrm{Re}(\mathbf{\Phi}) & -\mathrm{Im}(\mathbf{\Phi}) \\ \mathrm{Im}(\mathbf{\Phi}) & \mathrm{Re}(\mathbf{\Phi})\end{bmatrix}, \tag{23}$$

$$\mathbf{F} = \mathrm{diag}(\alpha_1, \ldots, \alpha_G, \alpha_1, \ldots, \alpha_G). \tag{24}$$

It is noted that, the real and imaginary parts share the same $\boldsymbol{\alpha}$ to ensure their group sparsity. The mean and variance of each scattering coefficients can be derived, once we obtain $\boldsymbol{\alpha}$ and β_0, which is determined by maximizing the logarithm of the marginal likelihood [30]. Then, the corresponding joint angle-range of targets, $(\theta_q, R_q), q = 1, \ldots, Q$, can be estimated by positions of the nonzero entries in $\mathbf{r}$.

IV. Simulation Results

For illustrative purposes, we consider an FDA radar exploiting coprime array and coprime frequency offset, where $M = 2$ and $N = 3$ are assumed. As shown in Fig. 2, the array and frequency offset consist of $(2M + N - 1) = 6$ physical elements, yielding $(3MN + M - N) = 17$ lags, respectively. As such, the increased number of DOFs can be used to localize far more targets than the number of array sensors as well as frequencies. In addition, the unit interelement spacing is $d = \lambda_0/2$, where λ_0 is the wavelength with respect to the carrier frequency $f_0 = 1$ GHz. We choose the unit frequency increment to be $\Delta f = 30$ KHz, resulting maximum unambiguous range $R_{\max} = c/(2\Delta f) = 5000$ m. In all simulations, Q far-field targets with identical powers are considered. The qth target is assumed to be on angle-range plane (θ_q, R_q), where $\theta_q \in [-60°, 60°]$ and $R_q \in [1000, 5000]$ m, for $q = 1, \cdots, Q$. The covariance matrix are obtained by using 1000 snapshots in the presence of noise with a 0 dB SNR.

In Fig. 3, we first compare the performance of different algorithms under 6 antennas and 6 frequencies, i.e., MUSIC algorithm with uniform linear arrays and uniform frequency offset (ULA-UFO), MUSIC algorithm with coprime arrays and coprime frequency offset (CA-CFO), and CMT-BCS with CA-CFO. Note that, spatial smoothing technique is applied to the covariance matrix so that its rank can be restored in MUSIC with CA-CFO. Thus, only consecutive lags can be used so that every sub-matrix has similar manifold. In Fig. 3(a), $Q = 9$ targets are selected, and the corresponding localization performance are illustrated in Figs. 3(b)–(d), respectively. It is evident that the cases of CA-CFO have better resolution than the ULA-UFO scenario for closely spaced targets by using virtual array and frequency. As a comparison, the CMT-BCS method outperforms the MUSIC algorithm, since it exploits all unique lags to form a virtual array and frequency, which yields larger array aperture and frequency increment than the corresponding MUSIC techniques using consecutive lags.

In the next example, $Q = 42$ targets, which is more than the available DOFs for the conventional FDA radar with ULA-UFO, are considered in Fig. 4. It is evident that all 42 targets can be localized using CMT-BCS with CA-CFO technique. Thus, the proposed approach enables localize more targets.

V. Conclusions

In this paper, we proposed a novel sparsity-based multi-target localization algorithm, which incorporates both coprime arrays and coprime frequency offsets in FDA radar platforms. By exploiting a sparse array and a frequency offset under the difference coarray equivalence, the proposed technique achieved a higher number of degrees-of-freedom representing a larger array aperture and increased frequency increments. These attributes enable high resolution localization of many more targets than the number of physical sensors. The effectiveness of the proposed technique was demonstrated by simulation results.

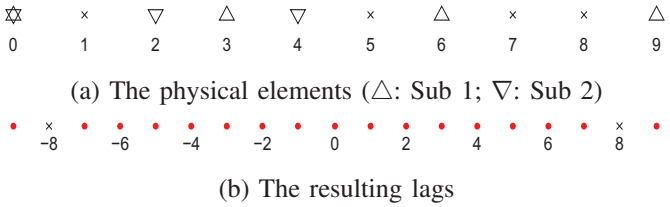

(a) The physical elements (△: Sub 1; ▽: Sub 2)

(b) The resulting lags

Fig. 2. The physical elements and corresponding lags.

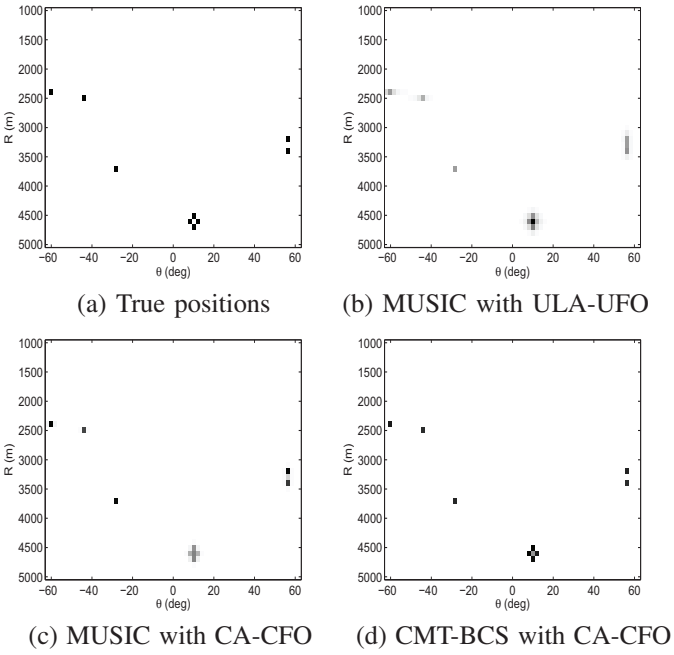

(a) True positions (b) MUSIC with ULA-UFO

(c) MUSIC with CA-CFO (d) CMT-BCS with CA-CFO

Fig. 3. The localization results using different approaches ($Q = 9$).

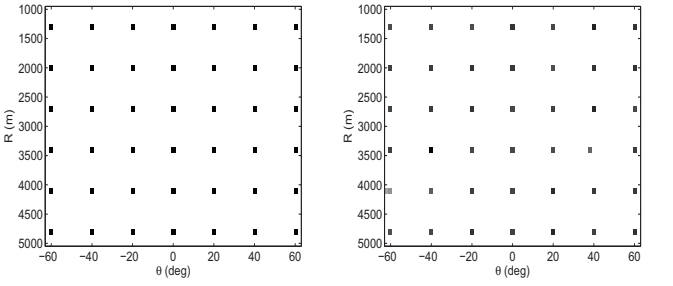

(a) True positions (b) CMT-BCS with CA-CFO

Fig. 4. The localization results using CMT-BCS with CA-CFO ($Q = 42$).

References

[1] M. Skolnik, *Radar Handbook, Third Edition*. McGraw-Hill, 2008.

[2] D. Ribas and P. Ridao, *Underwater SLAM for Structured Environments Using an Imaging Sonar*. Springer, 2010.

[3] G. Mao and B. Fidan, Eds, *Localization Algorithms and Strategies for Wireless Sensor Network*. Information Science Reference 2009.

[4] C. Gentile and N. Alsindi, *Geolocation Techniques: Principles and Applications*. Springer, 2012.

[5] Y. Zhang, X. Li, and M. G. Amin, "Principles and techniques of RFID positioning," in M. Bolic, D. Simplot-Ryl, and I. Stojmenovic (eds.), *RFID Systems, Research Trends and Challenges*. John Wiley, 2010.

[6] Y. Zhang, M. G. Amin, and S. Kaushik, "Localization and tracking of passive RFID tags based on direction estimation," *Int. J. Antennas Propagat.*, vol. 2007, Article ID 17426, doi:10.1155/2007/17426, 9 pages, 2007.

[7] B. K. Chalise, Y. D. Zhang, M. G. Amin, and B. Himed, "Target localization in a multi-static passive radar system through convex optimization," *Signal Process.*, vol. 102, pp. 207-215, 2014.

[8] I. Bekkerman and J. Tabrikian, "Target detection and localization using MIMO radars and sonars," *IEEE Trans. Signal Process.*, vol. 54, no. 10, pp. 3873–3883, 2006.

[9] Y. Zhang, M. G. Amin, and F. Ahmad, "Time-frequency analysis for the localization of multiple moving targets using dual-frequency radars," *IEEE Signal Process. Lett.*, vol. 15, pp. 777-780, 2008.

[10] H. Yan, J. Li, and G. Liao, "Multitarget identification and localization using bistatic MIMO radar systems," *EURASIP J. Adv. Signal Process.*, vol. 2008, no. ID 283483, 2008.

[11] P. Antonik, M. C. Wicks, H. D. Griffiths, and C. J. Baker, "Frequency diverse array radars," in *Proc. IEEE Radar Conf.*, Verona, NY, 2006, pp. 215–217.

[12] M. Secmen, S. Demir, A. Hizal, and T. Eker, 'Frequency diverse array antenna with periodic time modulated pattern in range and angle," in *Proc. IEEE Radar Conf.*, Boston, MA, 2007, pp. 427–430.

[13] P. Antonik, "An investigation of a frequency diverse array," Ph.D. dissertation, Univ. College London, London, U.K., 2009.

[14] W. Q. Wang, "Frequency diverse array antenna: new opportunities," *IEEE Antennas Propagat. Mag.*, vol. 57, no. 2, pp. 145–152, 2015.

[15] R. T. Hoctor and S. A. Kassam, "The unifying role of the coarray in aperture synthesis for coherent and incoherent imaging," *Proc. IEEE*, vol. 78, no. 4, pp. 735–752, 1990.

[16] W. Q. Wang, H. C. So, and H. Shao, "Nonuniform frequency diverse array for range-angle imaging of targets," *IEEE Trans. Signal Process.*, vol. 62, no. 8, pp. 2000–2011, 2011.

[17] P. P. Vaidyanathan and P. Pal, "Sparse sensing with co-prime samplers and arrays," *IEEE Trans. Signal Process.*, vol. 59, no. 2, pp. 573-586, 2011.

[18] P. Pal and P. P. Vaidyanathan, "Coprime sampling and the MUSIC algorithm," in *Proc. IEEE Digital Signal Process. Workshop and IEEE Signal Process. Educ. Workshop*, Sedona, AZ, 2011, pp. 289–294.

[19] Y. D. Zhang, M. G. Amin, F. Ahmad, and B. Himed, "DOA estimation using a sparse uniform linear array with two CW signals of co-prime frequencies," in *Proc. IEEE Workshop Comput. Adv. Multi-sensor Adapt. Process.*, Saint Martin, 2013, pp. 404–407.

[20] S. Qin, Y. D. Zhang, and M. G. Amin, "DOA estimation exploiting coprime frequencies," in *Proc. SPIE Wireless Sens., Localization, Process. Conf.*, Baltimore, MD, 2014, vol. 9103, pp. 91030E1–91030E7.

[21] C. L. Liu and P. P. Vaidyanathan, "Coprime arrays and samplers for space-time adaptive processing," in *Proc. IEEE Int. Conf. Acoust. Speech Signal Process.*, Brisbane, Australia, 2015, pp. 2364–2368.

[22] S. Qin, Y. D. Zhang, and M. G. Amin, "High-resolution frequency estimation using generalized coprime sampling," in *Proc. SPIE Wireless Sens., Localization, Process. Conf.*, Baltimore, MD, 2015, vol. 9497, pp. 94970K1–94970K7.

[23] Q. Wu and Q. Liang, "Coprime sampling for nonstationary signal in radar signal processing," *EURASIP J. Wireless Commun. Netw.*, doi:10.1186/1687–1499–2013–58, 2013.

[24] J. Chen, Q. Liang, B. Zhang and X. Wu, "Specturm efficiency of nested sparse sampling and co-prime sampling,'" *EURASIP J. Wireless Commun. Netw.*, doi:10.1186/1687–1499–2013–47, 2013.

[25] K. Adhikari, J. R. Buck and K. E. Wage, "Extending coprime sensor arrays to achieve the peak side lobe height of a full uniform linear array," *EURASIP J. Wireless Commun. Netw.*, doi:10.1186/1687–6180–2014–148, 2014.

[26] S. Qin, Y. D. Zhang, and M. G. Amin, "Generalized coprime array configurations for direction-of-arrival estimation," *IEEE Trans. Signal Process.*, vol. 63, no. 6, pp. 1377–1390, 2015.

[27] S. Qin, Y. D. Zhang, M. G. Amin, and A. Zoubir "Generalized coprime sampling of Toeplitz matrices," in *Proc. IEEE Int. Conf. Acoust. Speech Signal Process.*, Shanghai, China, 2016.

[28] D. L. Donoho, "Compressed sensing," *IEEE Trans. Inf. Theory*, vol. 52, no. 4, pp. 1289-1306, 2006.

[29] S. Qin, Y. D. Zhang, and M. G. Amin, "Sparsity-based multi-target localization exploiting multi-frequency coprime array," in *Proc. IEEE ChinaSIP*, Chengdu, China, 2015, pp. 329–333.

[30] Q. Wu, Y. D. Zhang, and M. G. Amin, "Complex multitask Bayesian compressive sensing," in *Proc. IEEE Int. Conf. Acoust. Speech Signal Process.*, Florence, Italy, 2014, pp. 3375–3379.

[31] R. Klemm, *Space-Time Adaptive Processing: Principles and Applications*. IEEE Press, 1998.

[32] Y. M. Chen, "On spatial smoothing for two-dimensional direction-of-arrival estimation of coherent signals," *IEEE Trans. Signal Process.*, vol. 45, no. 7, pp. 1689–1696, 1997.

[33] S. S. Chen, D. L. Donoho, and M. A. Saunders, "Atomic decomposition by basis pursuit," *SIAM J. Sci. Comput.*, vol. 20, no. 1, pp. 33–61, 1998.

[34] J. A. Tropp and A. C. Gilbert, "Signal recovery from random measurements via orthogonal matching pursuit," *IEEE Trans. Inf. Theory*, vol. 53, no. 12, pp. 4655–4666, 2007.

[35] S. Ji, Y. Xue, and L. Carin, "Bayesian compressive sensing," *IEEE Trans. Signal Process.*, vol. 56, no. 6, pp. 2346–2356, Aug. 2008.

[36] S. Ji, D. Dunson, and L. Carin, "Multitask compressive sensing," *IEEE Trans. Signal Process.*, vol. 57, no. 1, pp. 92–106, 2009.

[37] Q. Wu, Y. D. Zhang, M. G. Amin, and B. Himed, "Multi-task Bayesian compressive sensing exploiting intra-task correlation," *IEEE Signal Process. Lett.*, vol. 22, no. 4, pp. 430–434, 2015.

[38] M. E. Tipping, "Sparse Bayesian shrinkage and selection learning and the relevance vector machine," *J. Mach. Learn. Res.*, vol. 1, no. 9, pp. 211–244, 2001.